

High-Spin Ferric Ions in *Saccharomyces cerevisiae* Vacuoles Are Reduced to the Ferrous State during Adenine-Precursor Detoxification

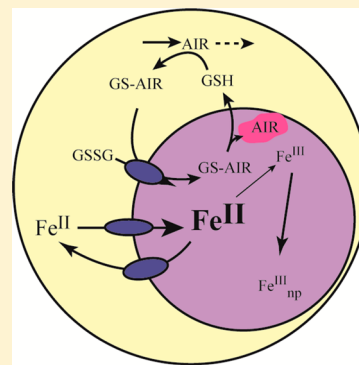
Jinkyu Park,^{†,‡} Sean P. McCormick,[†] Allison L. Cockrell,[‡] Mrinmoy Chakrabarti,[†] and Paul A. Lindahl*,^{†,‡}

[†]Department of Chemistry, Texas A&M University, College Station, Texas 77843-3255, United States

[‡]Department of Biochemistry and Biophysics, Texas A&M University, College Station, Texas 77843-2128, United States

Supporting Information

ABSTRACT: The majority of Fe in Fe-replete yeast cells is located in vacuoles. These acidic organelles store Fe for use under Fe-deficient conditions and they sequester it from other parts of the cell to avoid Fe-associated toxicity. Vacuolar Fe is predominantly in the form of one or more magnetically isolated nonheme high-spin (NHHS) Fe^{III} complexes with polyphosphate-related ligands. Some Fe^{III} oxyhydroxide nanoparticles may also be present in these organelles, perhaps in equilibrium with the NHHS Fe^{III}. Little is known regarding the chemical properties of vacuolar Fe. When grown on adenine-deficient medium (A↓), ADE2Δ strains of yeast such as W303 produce a toxic intermediate in the adenine biosynthetic pathway. This intermediate is conjugated with glutathione and shuttled into the vacuole for detoxification. The iron content of A↓ W303 cells was determined by Mössbauer and EPR spectroscopies. As they transitioned from exponential growth to stationary state, A↓ cells (supplemented with 40 μM Fe^{III} citrate) accumulated two major NHHS Fe^{II} species as the vacuolar NHHS Fe^{III} species declined. This is evidence that vacuoles in A↓ cells are more reducing than those in adenine-sufficient cells. A↓ cells suffered less oxidative stress despite the abundance of NHHS Fe^{II} complexes; such species typically promote Fenton chemistry. Most Fe in cells grown for 5 days with extra yeast-nitrogen-base, amino acids and bases in minimal medium was HS Fe^{III} with insignificant amounts of nanoparticles. The vacuoles of these cells might be more acidic than normal and can accommodate high concentrations of HS Fe^{III} species. Glucose levels and rapamycin (affecting the TOR system) affected cellular Fe content. This study illustrates the sensitivity of cellular Fe to changes in metabolism, redox state and pH. Such effects broaden our understanding of how Fe and overall cellular metabolism are integrated.



Iron (Fe) serves many essential roles in cell biology. This redox-active transition metal functions in enzyme catalysis, electron-transfer processes, and small-molecule binding and activation.¹ It is found as Fe/S clusters (ISCs), heme centers, nonheme mono- and dinuclear complexes, among others. Nonheme high-spin (NHHS) Fe^{II} complexes generally promote Fenton chemistry, which can be detrimental to the cell; such complexes help generate reactive oxygen species (ROS), which can damage DNA, proteins, and membranes. Thus, Fe trafficking, regulation, and sequestration are important aspects of cellular Fe metabolism.

The molecular-level details of Fe metabolism in eukaryotes are best understood in the budding yeast *Saccharomyces cerevisiae*.^{2,3} Numerous proteins on the plasma membrane of this organism import Fe from the environment. The membrane-bound Fet3p/Ftr1p (ferroxidase/permease) complex constitutes the “high-affinity” Fe importer,⁴ whereas Fet4p and/or Smf1p constitute “low-affinity” importers.^{5,6} The genes encoding the high-affinity importer and about 20 other Fe-related proteins in the cell are regulated by Aft1p.⁷ Under low-Fe conditions, this transcription factor moves to the nucleus where it activates these genes. Under Fe-replete conditions, Aft1p is deactivated and it moves into the cytosol in an Fe-

dependent process that involves binding to the [Fe₂S₂]-containing Grx3/4p-Fra2p heterodimer.^{8,9}

Mitochondria are the primary sites in the cell for ISC assembly and the only site of heme biosynthesis. Cytosolic Fe is imported into this organelle via the inner-membrane proteins Mrs3p/4p; these proteins constitute the primary mitochondrial Fe import pathway. Secondary pathways also exist but are less well characterized.^{10,11} Many nascent ISCs and hemes are installed into respiratory complexes and other respiration-associated mitochondrial proteins.

Vacuoles sequester, store, and mobilize Fe as needed by the cell. Under standard conditions, the vacuoles are acidic, with pH ~ 5.¹² The dominant form of Fe in these organelles is one or more NHHS magnetically isolated Fe^{III} complex(es) with polyphosphate-related ligands.¹³ Under Fe-replete growth conditions (>10 μM Fe), vacuolar Fe constitutes the majority of cellular Fe, with mitochondrial Fe constituting much of the remainder.¹⁴ Other forms of Fe, for example, those found in the

Received: February 3, 2014

Revised: May 13, 2014

Published: June 11, 2014

cytosol, appear to compose less than ~10% of the total Fe in Fe-replete WT cells. The acidity of the vacuoles plays an important role in Fe homeostasis. When vacuoles become less acidic, the Fe regulon is activated, and additional vacuolar Fe is imported.^{15,16} This may arise from the accumulation of Fe^{III} nanoparticles in these organelles, which form under alkaline conditions.^{13,17}

Many strains of *S. cerevisiae*, including that used in our studies (W303), contain a mutation in *ADE2*, a gene required for adenine biosynthesis. Minimal medium (MM) contains sufficient adenine such that MM-grown cells are adenine-replete. However, cells grown in medium containing insufficient adenine make a futile attempt to synthesize the purine. Instead, they synthesize and accumulate a toxic intermediate, 5-aminoimidazole ribotide (AIR), which is sequestered into vacuoles. To do this, the cell attaches glutathione to an activated form of AIR^{18,19} affording a glutathione conjugate (GS-X) that is pumped into vacuoles via ABC transporters on the vacuolar membrane. Such pumps include Ycf1p, Ybt1p, and Bat1p, with Ycf1p playing the dominant role.^{19–21} Once in the vacuole, the conjugate is degraded and an aggregated pink derivative of AIR accumulates. Freed glutathione in the vacuole is hydrolyzed by γ -glutamyl transpeptidase and L-Cys-Gly dipeptidase, forming glutamate, glycine and cysteine, which are returned to the cytosol.²²

The redox status of the cell is largely determined by the glutathione/glutaredoxin (and thioredoxin-based) systems.²³ A 10 mM glutathione (GSH) pool in the cytosol along with the low concentration of oxidized glutathione disulfide (the molar GSH:GSSG ratio is estimated at 50,000:1) establish the redox potential of this cellular region.²⁴ Ycf1p, the main vacuolar transporter that pumps glutathione conjugates into these organelles, functions to maintain this ratio by pumping GSSG into vacuoles. Doing so raises the redox potential of the vacuoles as it lowers that of the cytosol.

We report here that the Fe^{III} polyphosphate-related complex(es) in the vacuole become(s) reduced to the Fe^{II} state in adenine-deficient cells. This effect is undoubtedly associated with the detoxification of AIR. The effect is transient, with Fe^{II} reverting back to Fe^{III} when cells reach the postexponential stage of growth. Loss of acidic conditions promotes the formation of nanoparticles, whereas highly acidic conditions maintain the Fe in a mononuclear Fe^{III} state. Such redox- and pH-dependent activities have not been described for vacuolar Fe. We demonstrate that vacuolar Fe^{III} is not “locked” into the oxidized mononuclear state but rather can be reversibly reduced and reoxidized and converted into nanoparticles. These transformations depend on the redox and pH status of the vacuole. Changing the nutrient composition in other ways (glucose, yeast-nitrogen-base, amino acids, and nucleotide bases) also impacted the Fe content of yeast cells. We also examined the effect of inhibiting the Target of Rapamycin Complex 1 (TORC1). TORC1 is central to a partially defined metabolic system, the inhibition of which is associated with the starvation response, including increased lifespan.²⁵ Although the molecular-level causes of such effects are unknown, they illustrate the complex relationship between Fe and overall cellular metabolism.

EXPERIMENTAL PROCEDURES

Yeast Strain and Media. The main strain used in this study was W303-1B (*MATα, ura3-1, ade2-1, trp1-1, his3-11,15, leu2-3,112*) purchased from American Type Culture Collection

(ATCC). Stocks were prepared by growing cells for 3–4 days on agar plates consisting of standard rich medium with 2% (w/v) glucose and 40 mg/L adenine hemisulfate dihydrate (YPAD). Cells were removed from the plate, resuspended in 15% glycerol, and stored at –80 °C.

As needed, frozen cells were scraped with a sterile wooden stick and spread onto an agar plate. Typically a single colony was used to inoculate 50 mL of YPD medium. Cells were grown to OD₆₀₀ ≈ 1 and then transferred to 200 mL of synthetic medium. MM consisted of 1.7 g/L YNB (MP biomedical #4027-112, which lacked (NH₄)₂SO₄, FeCl₃, and CuSO₄), 38 mM (NH₄)₂SO₄, 1 μM CuSO₄, 2% (w/v) glucose, 0.76 mM leucine, 0.13 mM histidine, 0.24 mM tryptophan, 0.10 mM adenine hemisulfate dihydrate, and 0.18 mM uracil. R+ medium was prepared by adding a solution of rapamycin, dissolved in DMSO, to MM (20 nM final concentration). ⁵⁶Fe- or ⁵⁷Fe-citrate was added separately, to 40 μM final concentration. Adenine-deficient MM (A↓) was the same as MM except that it contained 12 μM adenine unless otherwise indicated. YAB↑ medium was the same as MM except that it contained 3× more YNB, 3× more of the three Amino acids Leu, His, and Trp, and 3× more of the Bases adenine and uracil. Cells were grown on 200 mL of MM and YAB↑ media in 1 L baffled culture flasks starting at an OD₆₀₀ ≈ 0.01. Cells were also grown on 1 L of A↓ medium in 3.8 L baffled culture flasks starting at the same OD₆₀₀.

Cells were grown for 5 days in a shaker at ~150 rpm and 30 °C. Growth was monitored at OD₆₀₀. Cells were typically harvested at 1 and 5 days. Cells were processed for metal analysis, stored at –80 °C for later Oxyblot analysis, or packed into MB cups or EPR tubes as described.²⁶

For fluorescent studies, 5 day MM and YAB↑ cells were washed with 10 mM HEPES buffer, pH 7.4, containing 5% glucose. Washed cells were pelleted at 5000g for 5 min and resuspended in fresh buffer containing 10 μM MDY-64 fluorescent probe (Molecular Probes, Oregon). After incubation for 5 min, cells were pelleted at 5000g for 5 min and resuspended in fresh buffer without probe. Suspensions were placed on poly-L-lysine treated slides and examined by a Zeiss 510 META NLO laser scanning microscope (Carl Zeiss Microimaging, Thornwood, NY). Cells were irradiated at an excitation wavelength of 451 nm; the emission intensity at 497 nm was measured. The diameters of 100 cells and their vacuoles from each growth condition were measured using ImageJ software.

Isolation of Mitochondria and Vacuoles. To isolate mitochondria, 50 mL of MM cell culture (OD₆₀₀ ~ 1) was transferred to 1 L MM. When the culture reached OD₆₀₀ ~ 1, it was used to inoculate 24 L of A↓ medium at 30 °C in a stirred glass fermenter. The same procedure was followed for isolating vacuoles, except that 48 L of A↓ medium was used. Solutions were purged with 99.6% O₂ at 2 L/min to achieve aerobic growth conditions. Cells were harvested after 24 h. Mitochondria and vacuoles were isolated in a refrigerated Atmosphere glovebox (MBraun, < 10 ppm of O₂) as described.^{13,27}

Preparation of Redox- and pH-Perturbed Cell Lysates. Cells were grown to OD₆₀₀ = 1 in MM. An aliquot (the first aliquot) of the culture was used to prepare whole-cell MB samples as described below. Three other aliquots were spun down at 2500g for 5 min and frozen at –80 °C. Frozen aliquots were treated as follows. The second aliquot was thawed in the refrigerated glovebox and mixed with 25 mM Tris–HCl buffer

(pH 7.4) containing 1% Triton-X at a 3:1 (cell: buffer, v/v) ratio. The mixture was incubated for 30 min and frozen in liquid N₂ in a MB cup. The third and fourth aliquots were thawed under O₂-dominating atmosphere and mixed with 0.5 M acetate, pH 4.5 plus 1% Triton-X buffer (final pH 5.0) and 0.5 M Tris-HCl pH 8.0 plus 1% Triton-X buffer (final pH 7.8), respectively. The buffers were oxygenated by bubbling with 99.6% O₂ for 15 min before mixing and the mixtures were also bubbled with O₂ for 15 min. The resultant lysates were frozen in MB cups using liquid N₂.

Mössbauer Spectroscopy. Isolated mitochondria, vacuoles, and whole cells were packed into MB cups by centrifugation at 18000g for 30 min, 10900g for 45 min, and 4000g for 5 min, respectively, using an ultracentrifuge (Beckman Coulter Optima L-90K) with a swinging-bucket rotor (SW 32 Ti). Samples were frozen in liquid N₂. MB spectra were recorded on a Model MS4 WRC spectrometer (SEE Co., Edina, MN) that had been calibrated using α -Fe foil as described.²⁷

UV-Vis Spectroscopy. Whole cells were packed into quartz EPR tubes (5.0 mm OD; 3.4 mm ID; 80 mm long; Wilmad/Lab Glass, Buena, NJ, U. S. A.) at 4000g for 5 min. They were resuspended with an equal volume of deionized water and analyzed as described.²⁶ Each sample was scanned six times and the results were averaged to improve the signal-to-noise ratio. Resultant absorbances were multiplied by 5 to generate those expected if a 10 mm, rather than 2 mm, path length cuvette had been used.

Iron Concentrations. Packed mitochondria, vacuoles, and whole cells were diluted 2–4 fold with deionized water. The resulting ca. 400 μ L suspensions were transferred to screw-top plastic tubes and heated at 95 °C overnight in 200 μ L of 30% trace-metal grade HNO₃ (Fisher Scientific). Fe concentrations were measured by ICP-MS (Agilent 7700x) as described.²⁶ Reported Fe concentrations of mitochondria, vacuoles, and whole cells were multiplied by dilution factors and adjusted using previously reported packing efficiencies of 0.77 for mitochondria, 0.76 for vacuoles, and 0.70 for whole cells.^{13,28}

Oxyblot Assay. Whole-cell lysates were analyzed using the Oxyblot assay kit (Millipore) as described.²⁶ Protein concentrations in lysates were measured using the BCA protein assay kit (Pierce). Blot densities on membranes were quantified by using ImageJ software (NIH).

RESULTS

Adenine Deficiency. W303 cells in adenine-deficient minimal medium (called A↓ cells) grew exponentially at the same rate (doubling time ≈ 2.0 h) as cells grown on MM (Figure 1B, solid and open circles, respectively, from 0–10 h). Exponentially growing A↓ cells were *not* pink, indicating that they were not adenine deficient. An electronic absorption spectrum of such cells exhibited peaks due to reduced heme centers (Figure 1C, I). A↓ cells harvested during this period ($OD_{600} = 0.3$) contained $390 \pm 110 \mu\text{M}$ Fe.

When growth was started at the same OD, the growth of A↓ cells slowed earlier than that of MM cells; they also transitioned earlier into stationary state (Figure 1B, starting at ~12 h, $OD_{600} = 0.5$). As they transitioned, A↓ cells turned pink, indicating that the AIR-associated pigment in the vacuole was accumulating. The electronic absorption spectrum of such cells contained absorption maxima at 490 and 540 nm (Figure 1C, II), as published for adenine-deficient cells.¹⁸ A↓ cells probably transitioned earlier from exponential growth mode

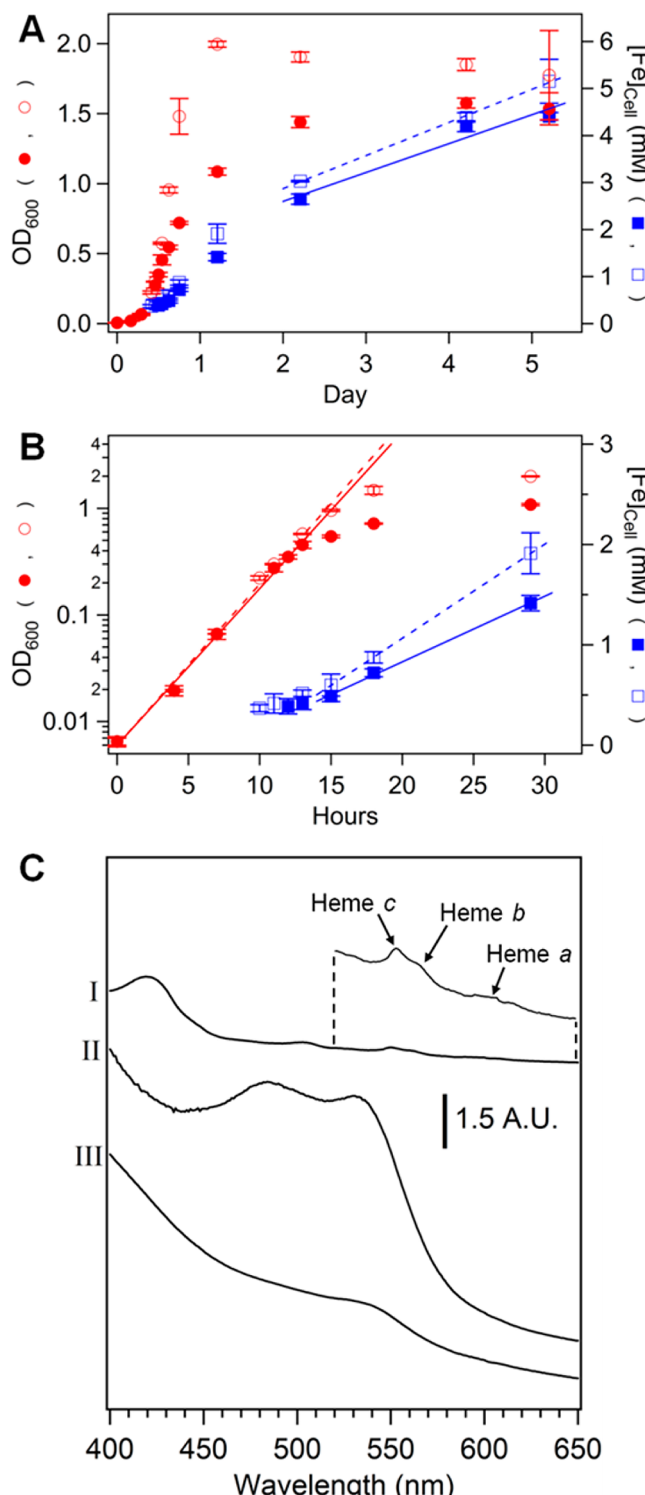


Figure 1. Plots of W303 cell growth on MM and A↓ media. (A) OD₆₀₀ (circles) and Fe concentration (squares). Open symbols, MM; solid symbols, A↓. Dashed and solid blue lines indicate Fe accumulation during stationary growth mode of MM and A↓ cells, respectively. MM data were from a previous study.¹⁷ Plots are the averages of two independent experiments; vertical bars indicate standard deviation. (B) Zoom of initial 30 h in (A). Dashed (MM) and solid (A↓) lines represent OD₆₀₀ trend lines in log scale during exponential growth (in red) and Fe accumulation trend lines during transitional growth (in blue). (C) UV-vis spectra of A↓ cells. I, OD₆₀₀ = 0.2, 8 h; II, OD₆₀₀ = 1.3, 1 day; III, OD₆₀₀ = 2.1, 5 days (10-fold diluted). Inset, same as I but magnified to show heme features better.

because they experienced a shortage of adenine. The intensity of the pink color increased during the transitional growth period. In the stationary state, cells were dark magenta, implying that the pigment that accumulated during the transitional period did not decompose in the stationary state. After 5 days of growth, the electronic absorption spectrum of A↓ cells was dominated by a broad absorption/scattering feature that was probably due to thickening of cell walls with aging (Figure 1C, III).

MM cells accumulate Fe as they transition from exponential growth to stationary state (Figure 1, A and B, open squares); this occurs because the Fe import rate declines more slowly than the growth rate declines.¹⁷ A↓ cells also accumulated Fe during the transitional period (Figure 1, solid squares) but at a slower rate (70 vs. 100 μM/h, solid vs. dashed lines between 15–30 h in Figure 1B). A↓ cells harvested during late transitional growth (after 29 h of growth) contained 1.4 ± 0.1 mM Fe ($n = 2$), which was slightly lower than equivalent MM cells (1.9 ± 0.1 mM). This suggests that the declining Fe import and growth rates were better synchronized in A↓ cells than in MM cells during this transition.

During the stationary state, both MM and A↓ cells accumulated Fe at similar rates, namely 30 vs 25 μM/h, respectively (Figure 1A, dashed vs solid lines at $t > 2$ days). These rates were probably associated with the unregulated import of Fe through the low-affinity import system.¹⁷ After 5 days of growth, A↓ cells contained 4.4 ± 0.1 mM Fe, whereas equivalently grown MM cells contained 5.2 ± 0.5 mM Fe (Supporting Information Table S1).

What type of Fe did A↓ cells contain? When harvested during early exponential phase ($OD_{600} = 0.2$), they exhibited a low-temperature low-field Mössbauer (MB) spectrum similar to that of MM cells (Figure 2, A vs. B). Dominating both spectra was a sextet due to vacuolar HS Fe^{III}; this was simulated by the purple line above the spectrum in Figure 2A. The central doublet (CD) was simulated by the green line. The CD is due to $[Fe_4S_4]^{2+}$ clusters and low-spin (LS) Fe^{II} hemes; the two types of centers cannot be resolved by MB spectroscopy.

A↓ cells harvested during the transitional period (after 1 day of growth) exhibited a MB spectrum that was dominated, with 56% spectral intensity, by a broad NHHS Fe^{II} doublet (Figure 2C). In contrast, MM cells mostly accumulated Fe^{III} oxyhydroxide nanoparticles (with a small amount of NHHS Fe^{II}) as they transitioned to stationary state (Figure 2D). A sextet originating from vacuolar HS Fe^{III} ions was also present in the spectrum of A↓ cells, but at ca. half the normal intensity (31%). In 3 other independent batches of A↓ cells (Figure 3, data compiled in Supporting Information Table S2), the percentage of the NHHS Fe^{II} doublet in MB spectra was as high as 84% and that of the NHHS Fe^{III} sextet was as low as 7%. The concentration of NHHS Fe^{II} in A↓ cells (total $[Fe_{cell}] = 780 \mu M$) harvested during the transitional period was about 430 μM. To put this into perspective, the concentration of such species in adenine-sufficient cells ranges from 20–70 μM.^{14,26,28}

The difference-spectrum (Figure 2E) revealed that the Fe that accumulated during the transitional growth period of A↓ cells was mainly NHHS Fe^{II} (85%, maroon and yellow lines), along with a small contribution of Fe^{III} nanoparticles (10%, blue line). The CD concentration slightly declined as A↓ cells entered the transitional phase (Figure 2E, green line). This suggests a decline in mitochondrial Fe; however, the two samples that were used to generate this difference-spectrum were from different batches and there might have been some

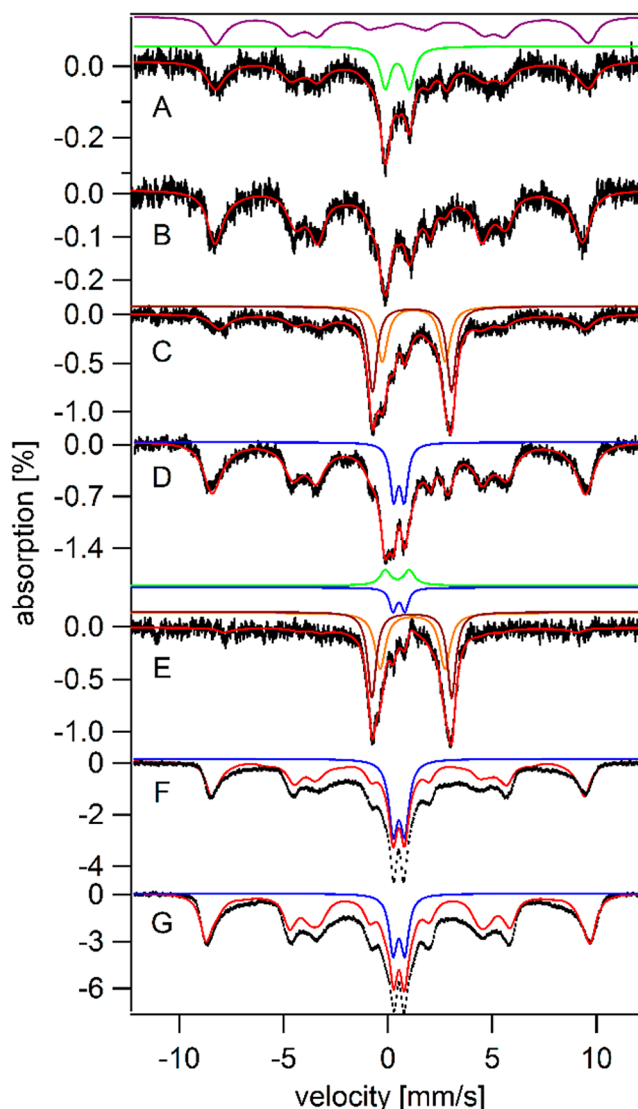


Figure 2. Five K, 0.05 T Mössbauer spectra of A↓ and MM cells, harvested at different growth phases. A, A↓, exponential ($OD_{600} = 0.2$); B, MM, exponential ($OD_{600} = 0.2$); C, A↓, transitional ($OD_{600} = 0.9$); D, MM, transitional ($OD_{600} = 1.8$); E, C-minus-A difference spectrum; F, A↓, 5-day stationary ($OD_{600} = 0.9$); G, MM, 5-day stationary ($OD_{600} = 1.8$). Red lines are composite simulations that include NHHS Fe^{III}, NHHS Fe^{II}, Fe^{II} heme, CD, and Fe^{III} nanoparticle features. The purple, green and blue lines are simulations of the NHHS Fe^{III}, CD and Fe^{III} nanoparticle spectral features, respectively. Maroon and orange lines in C and E are simulations of the Fe^{II}_{ONS} and Fe^{II}_{ON} doublets, respectively. Parameters used in simulations are given in Supporting Information Table S2.

batch-to-batch variation in the level of mitochondria. The MB spectrum of mitochondria isolated from A↓ cells exhibited a strong CD (Figure 4A, green line), providing no evidence that A↓ cells contain less CD-associated Fe than adenine-sufficient MM cells. UV-vis spectroscopy could not be used to settle this issue, as the pink color obscured heme features.

The broadness of the NHHS Fe^{II} doublet in Figure 2C suggested more than one component. In spectra from three independent preparations (Figure 3, A–C), the resolution was slightly better—sufficient to unambiguously demonstrate the presence of two major species called Fe^{II}_{ON} ($\delta = 1.2\text{--}1.3 \text{ mm/s}$ and $\Delta E_Q = 3.0\text{--}3.1 \text{ mm/s}$) and Fe^{II}_{ONS} ($\delta \approx 1.1 \text{ mm/s}$ and

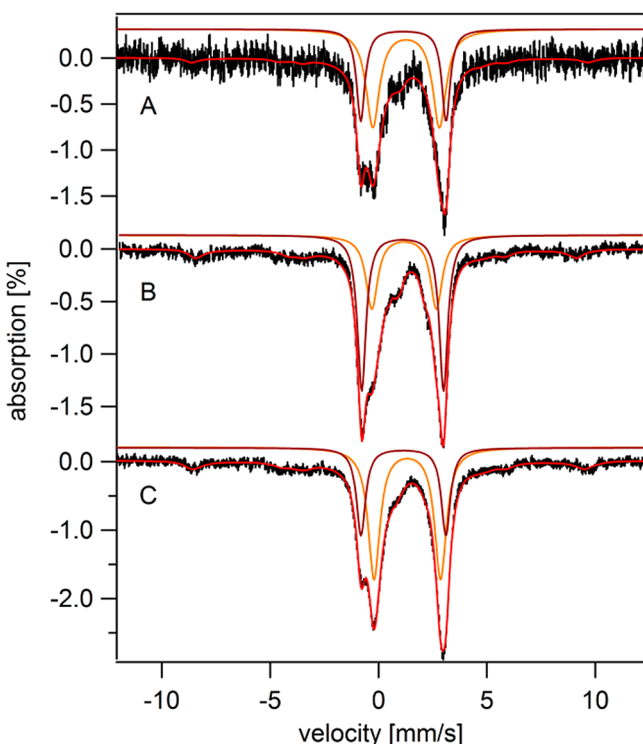


Figure 3. Five K, 0.05 T Mössbauer spectra of different A↓ cell batches at transitionary state. (A) A↓ cells harvested at $OD_{600} = 1.2$. (B) A↓ cells (with 25 μM adenine) harvested at $OD_{600} = 1.3$. (C) A↓ cells (with 25 μM adenine) harvested at $OD_{600} = 2.1$. Red lines are overall simulations. Maroon and orange lines simulate Fe^{II}_{ONS} and Fe^{II}_{ON} , respectively.

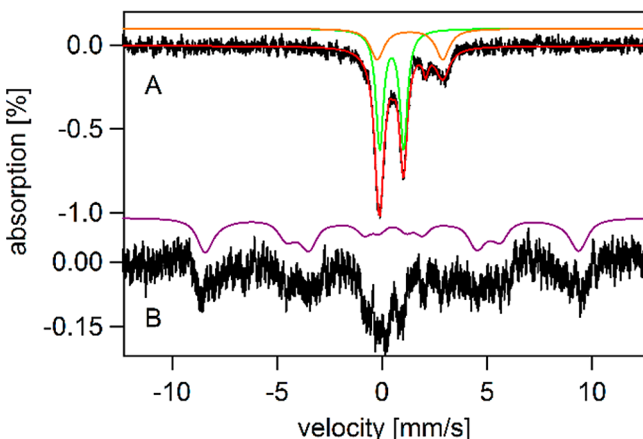


Figure 4. Five K, 0.05 T Mössbauer spectra of mitochondria (A) and vacuoles (B) isolated from 1 day-old A↓ cells ($OD_{600} = 0.9$). The red line simulates the major spectral features in (A), including the NHHS Fe^{II} doublet, the HS Fe^{II} heme doublet and the CD. The green line simulates the CD, whereas the orange and purple lines simulate the NHHS Fe^{III} and NHHS Fe^{II} species, respectively.

$\Delta E_Q = 3.8\text{--}3.9$ mm/s). Different batches contained different proportions of these two species. The parameters associated with Fe^{II}_{ON} suggest a 5- or 6-coordinate complex with O/N donors.²⁹ The parameters for Fe^{II}_{ONS} suggest somewhat greater covalency, possibly associated with coordination of a S-donor ligand. For example, the Fe^{II} ion in the active-site of isopenicillin N synthase has an N_2O_4 coordination sphere and exhibits a MB doublet with $\delta = 1.3$ mm/s and $\Delta E_Q = 2.7$

mm/s,^{30,31} arguably similar to the Fe^{II}_{ON} doublet. With substrate bound, the site becomes 5-coordinate with an $N_2O_2S_1$ donor set including thiolate ligation from the substrate. The associated MB doublet has $\delta = 1.1$ mm/s and $\Delta E_Q = 3.4$ mm/s, rather similar to the Fe^{II}_{ONS} doublet.³¹

Because the Fe concentrations of A↓ and adenine-sufficient MM cells harvested at this OD were similar, adenine deficiency appeared to cause the conversion of one form of cellular Fe into another rather than the import of new Fe. The simplest interpretation is that an adenine deficiency causes vacuoles to be more reduced such that vacuolar Fe^{III} (and/or Fe^{III} nanoparticles) is/are reduced to form the $Fe^{II}_{ON/S}$ species, perhaps occurring in association with ligand exchange.

The location(s) of Fe^{II}_{ON} and Fe^{II}_{ONS} is(are) unknown. The NHHS Fe^{II} doublet in the MB spectrum of isolated mitochondria (Figure 4A, simulated by the yellow line) was more intense than usual, but not enough to be responsible for the intense NHHS Fe^{II} doublets observed in the whole-cell spectrum (mitochondria represent only 3%–10% of the volume of a fermenting cell).³² MB spectra of vacuoles isolated from A↓ cells did not include the $Fe^{II}_{ON/S}$ doublets (Figure 4B), suggesting (but not proving) that these species are located elsewhere. Our hesitancy in concluding that $Fe^{II}_{ON/S}$ are not located in vacuoles is that vacuoles are highly dynamic, such that $Fe^{II}_{ON/S}$ could have exited the organelle during isolation. Although speculative, we currently regard the cytosol as the most likely location of Fe^{II}_{ON} and the vacuoles the most likely location of Fe^{II}_{ONS} . This assignment helps explain some data presented below.

Five-day-old A↓ cells harvested in stationary state were also pink (Figure 1C, III), but they contained far more Fe (4.4 mM) than did 1-day-old A↓ cells. This is slightly less than the Fe concentration of adenine-sufficient MM-grown cells harvested at an equivalent age (5.2 mM).¹⁷ Note that Fe concentrations in Supporting Information Table S1 were obtained from 200 mL cultures except A↓. For the same culture size A↓ cells accumulated slightly less Fe than MM cells.

The MB spectrum of 5-day-old A↓ cells (Figure 2F) was dominated by a sextet due to vacuolar HS Fe^{III} and a doublet due to Fe^{III} nanoparticles. The NHHS Fe^{II} doublets were dramatically reduced in intensity such that they could not be discerned in the spectrum. MM cells at the same age exhibited a very similar spectrum (Figure 2G). This indicates that the vacuole-reducing effect of adenine-deficiency was transient. When the cells reached stationary state, $Fe^{II}_{ON/S}$ must have been reoxidized back to what appears to be the same Fe^{III} species that is found in MM cells. In one of three batches of 5-day-old A↓ cells, the dominating HS Fe^{II} doublet was still observed by MB (Supporting Information Figure S1), indicating some batch-to-batch variation in the extent of reoxidation. Reoxidation may reflect a change in vacuolar/cytosolic redox state as the cells undergo the diauxic shift.

The spectrum of 5-day-old A↓ cells also contained a broad unresolved magnetic feature representing ~30% of the spectrum, again similar to that observed in the MB spectrum of 5-day-old MM cells.¹⁷ EPR of a corresponding A↓ sample exhibited a broad signal at $g = 2.0$ (Figure 5) that was similar to that observed in equivalent MM cells.¹⁷ The signal from MM cells originates from nanoparticles with somewhat different properties than those found in mitochondria of yeast strains with ISC defects.^{27,33,34}

A↓ cells harvested both at 1 and 5 days exhibited lower levels of oxidative stress relative to analogous MM cells (Figure 6,

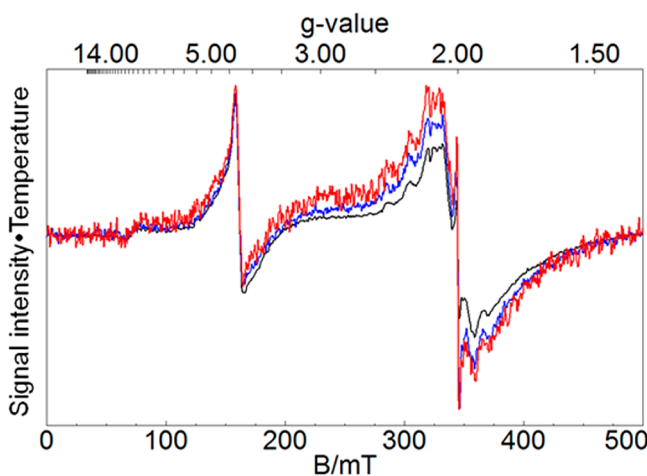


Figure 5. EPR spectra of $A\downarrow$ cells at stationary phase. Black, 10 K; blue, 30 K; red, 70 K. Spectra were recorded at 0.05 mW microwave power, 9.64 GHz frequency, and 10 G modulation amplitude. Spectral intensity was multiplied by temperature and then adjusted vertically to align the $g = 4.3$ resonances.

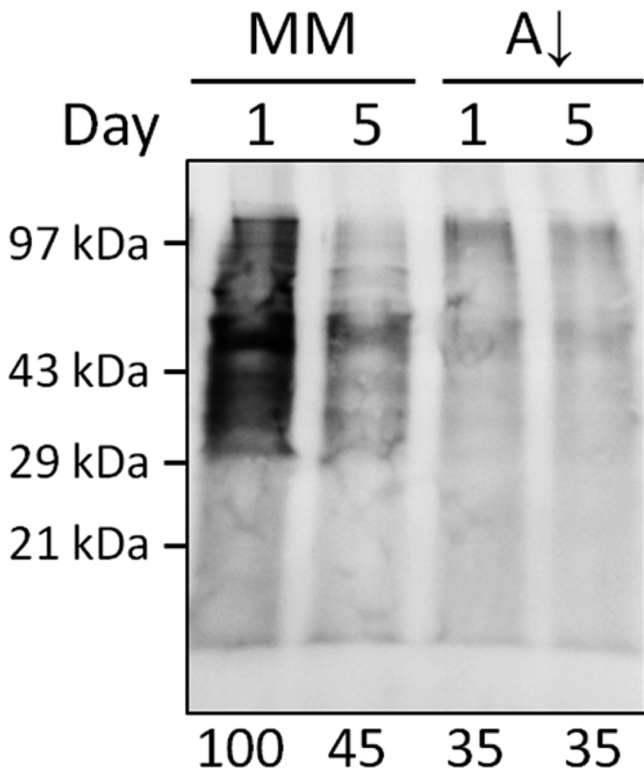


Figure 6. Oxyblot assay of MM and $A\downarrow$ extracts from cells harvested during different phases. Lane 1, MM, 1 day; lane 2, MM, 5 days; lane 3, $A\downarrow$, 1 day; lane 4, $A\downarrow$, 5 days. Percent band intensities relative to the blot from MM/1 day cells for each lane are displayed at the bottom of the image. Each lane contained 4 μ g of whole cell lysate protein.

lanes 3 and 4 vs lanes 1 and 2). The diminished degree of oxidative damage is consistent with a more reducing environment in the 1-day-old $A\downarrow$ cells but inconsistent with our expectation that high concentrations of NHHS $\text{Fe}^{\text{II}}_{\text{ON/S}}$ ions would promote oxidative damage. Such ions typically have labile ligands and can participate in Fenton chemistry.³⁵ This chemistry appears not to be occurring here. Also, the type of Fe, namely NHHS Fe^{II} in 1-day-old cells vs NHHS Fe^{III} and

nanoparticles in 5-day-old cells, does not seem to make much difference. Perhaps the level of oxidative stress is more closely correlated to the growth rate or redox state of the cell. The compartment in which the Fe accumulates might also matter; for example, Fe that accumulates in mitochondria might be more dangerous than Fe that accumulates in vacuoles. Further studies are required to investigate this.

Effect of Increasing Yeast-Nitrogen-Base, Amino Acids, and Nucleotide Bases in Growth Medium. We discovered that the chemical state of vacuolar Fe depends sensitively on the composition of the growth medium. The origin of these effects is uncertain, but they illustrate how Fe in the cell changes with metabolism. Cells grown on YAB↑ for 1 day exhibited a low-temperature low-field MB spectrum (Figure 7A) that was reminiscent of “young” MM cells (Figure 2B); in

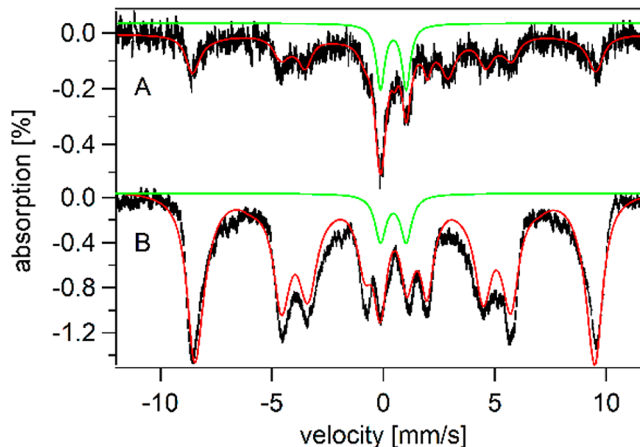


Figure 7. Five K, 0.05 T Mössbauer spectra of cells grown on YAB↑ media for 1 (A) and 5 (B) days. Green lines simulate the CD. Red lines are composite simulations.

both cases, the vacuolar NHHS Fe^{III} sextet dominated, followed by the CD. We suspect that the vacuoles are acidic in “young” cells. When grown for 5 days on YAB↑ medium, the cells exhibited MB spectra in which ~90% of the intensity was the vacuolar NHHS Fe^{III} sextet, with little or no nanoparticles (Figure 7B). In equivalent MM-grown cells (Figure 2G), the vacuolar NHHS Fe^{III} sextet represented just 65% of spectral intensity, with the nanoparticle doublet representing ~25%. Nanoparticles are generated from mononuclear Fe^{III} under neutral and basic pH conditions.¹³ Thus, the dominance of NHHS Fe^{III} and the absence of a nanoparticle doublet in spectra of YAB↑ cells suggest that the vacuoles in chronologically old YAB↑ cells remain acidic, whereas the pH of vacuoles in old MM-grown cells increased thereby causing nanoparticles to form.

Most of the remaining 10% intensity in spectra of YAB↑ cells originated from the CD (Figure 7B, green line). This corresponds to a CD concentration of 110 μM Fe, nearly 40% higher than that in MM-grown cells.¹⁷ Likewise, UV-vis spectra indicated that the concentration of Fe^{II} hemes in YAB↑ cells was 3-fold higher than in MM cells (Supporting Information Figure S2). Both results indicate that YAB↑ cells have a higher-than-normal level of mitochondrial Fe. This may reflect a greater reliance on respiration in these cells.

We previously estimated a maximum [Fe] in vacuoles of 1.2 mM and concluded that these organelles occupy no more than ~25% of the cell’s volume.¹³ Accordingly, filled vacuoles could

contribute a maximum of $\sim 300 \mu\text{M}$ to the total Fe concentration in MM cells. Contrasting this, YAB \uparrow cells at stationary state contained $1.8 \pm 0.1 \text{ mM Fe}$ ($n = 2$, Supporting Information Table S1), 90% of which was vacuolar NHHS Fe $^{\text{III}}$. If the vacuoles occupied 100% of the cell's volume, the concentration of Fe in this component would be 1.6 mM; if vacuoles still occupied $\sim 25\%$ of cell volume, the NHHS Fe $^{\text{III}}$ concentration in YAB \uparrow vacuoles would be nearly 6 mM!

To distinguish these possibilities, 5-day YAB \uparrow and MM cells were stained with a vacuole-specific fluorescent probe and examined by fluorescence microscopy. YAB \uparrow cells were slightly larger than MM cells (diameters of $6.1 \pm 0.8 \mu\text{m}$ and $5.2 \pm 0.8 \mu\text{m}$ ($n = 100$, each), corresponding to respective volumes of ~ 120 and 74 fL. The vacuoles in YAB \uparrow and MM cells represented $23\% \pm 6\%$ and $20\% \pm 8\%$ of cell volumes. This indicates that 5-day-old YAB \uparrow vacuoles contain very high concentrations of the NHHS Fe $^{\text{III}}$ species. Such highly acidic vacuoles may be able to store NHHS Fe $^{\text{III}}$ ions at concentrations approaching 6 mM.

Effect of Redox State and pH on Vacuolar Fe. To illustrate the effect of redox state and pH on the form of vacuolar Fe, these properties of whole-cell lysates were perturbed. Unperturbed WT cells grown on MM exhibited the standard MB spectrum (Figure 8A, similar to that in Figure 2A) composed predominantly of the vacuolar NHHS Fe $^{\text{III}}$

sextet (simulated by the purple line). A portion of these cells was disrupted by detergent treatment that caused vacuolar Fe to be exposed to the reducing environment of the cytosol. Approximately 70% of the Fe in the resulting lysate was NHHS Fe $^{\text{II}}$ (Figure 8B; yellow line simulates the doublet), implying that vacuolar Fe was reduced by endogenous cytosolic reducing agents. Simulation parameters were the same as those used to simulate Fe $^{\text{II}}_{\text{ONS}}$, not those of Fe $^{\text{II}}_{\text{ONs}}$. The formation of Fe $^{\text{II}}_{\text{ON}}$ under these conditions would imply a direct reduction of vacuolar iron ($\text{Fe}^{\text{III}}_{\text{vac}} + 1\text{e}^- \rightleftharpoons \text{Fe}^{\text{II}}_{\text{ON}}$). However, these simulation parameters are not unique to Fe $^{\text{II}}_{\text{ON}}$, so another (more complicated) scenario is also possible, namely that a different NHHS Fe $^{\text{II}}$ species with 5–6 O/N ligands formed. In either case, our results suggest that Fe $^{\text{II}}_{\text{ONS}}$ is more closely associated with adenine-deficiency, whereas Fe $^{\text{II}}_{\text{ON}}$ is more generally associated with reducing adenine-replete cellular conditions.

In cells that were lysed at pH 5.0 (final) under a pure O₂ atmosphere, half of the vacuolar Fe remained oxidized (Figure 8C), whereas in cells that were similarly lysed at pH 7.8 (final pH), at least half of the Fe converted into nanoparticles (Figure 8D). The remaining Fe exhibited an unresolved and broad feature that could reflect a different type of nanoparticle. The observed changes illustrate how redox and pH influence the state of vacuolar Fe.

Effect of Glucose. We wondered whether changing the composition of the growth medium in other ways would also alter cellular Fe content. Of all the nutrients in MM, glucose exerts perhaps the greatest influence on cellular metabolism.³⁶ Increasing the glucose concentration 3-fold (G \uparrow medium) did not affect the growth rate nor did it significantly affect the Fe concentration in cells harvested in stationary state (Supporting Information Table S1, G \uparrow vs MM). In contrast, lowering the glucose concentration 10-fold (G \downarrow medium) lowered the steady-state culture density by $\sim 40\%$ and lowered the cellular Fe concentration 7-fold (Supporting Information Table S1, G \downarrow vs MM). We conclude that glucose limited the growth in G \downarrow medium, whereas other nutrients limited the growth in G \uparrow medium.

The Fe concentrations of 1- and 5-day-old G \downarrow cells were nearly the same (940 vs 1000 μM) implying that the stationary-state Fe import rate through the low-affinity importer in G \downarrow cells was lower than in MM-grown cells. Perhaps this rate is glucose-dependent. In contrast, the rate of Fe import during exponential phase (through the high-affinity importer) was not affected by the glucose concentration. Under glucose-limited (G \downarrow) stationary state conditions, Fe is better regulated than in equivalent G \uparrow cells.

The speciation of Fe in G \uparrow cells was virtually identical to that of MM -cells (Figure 9, C vs B and Supporting Information Table S2); both were dominated by the vacuolar NHHS Fe $^{\text{III}}$ species (65% intensity) and Fe $^{\text{III}}$ nanoparticles (15–25% intensity). The distribution of Fe in G \downarrow cells (Figure 9A) was perhaps more similar to that in cells treated with rapamycin (Figure 9E, see below).

The proportion of Fe associated with mitochondria in G \downarrow and G \uparrow cells was difficult to evaluate in these MB experiments because the CD was obscured by the broad nanoparticle doublet and the strong sextet in that region of the spectrum. However, UV-vis spectra of these glucose-modulated cells (Figure 10, A–C) clearly indicated that heme concentrations (which primarily reflect mitochondrial respiratory complexes and respiration-associated heme proteins) were higher in G \downarrow

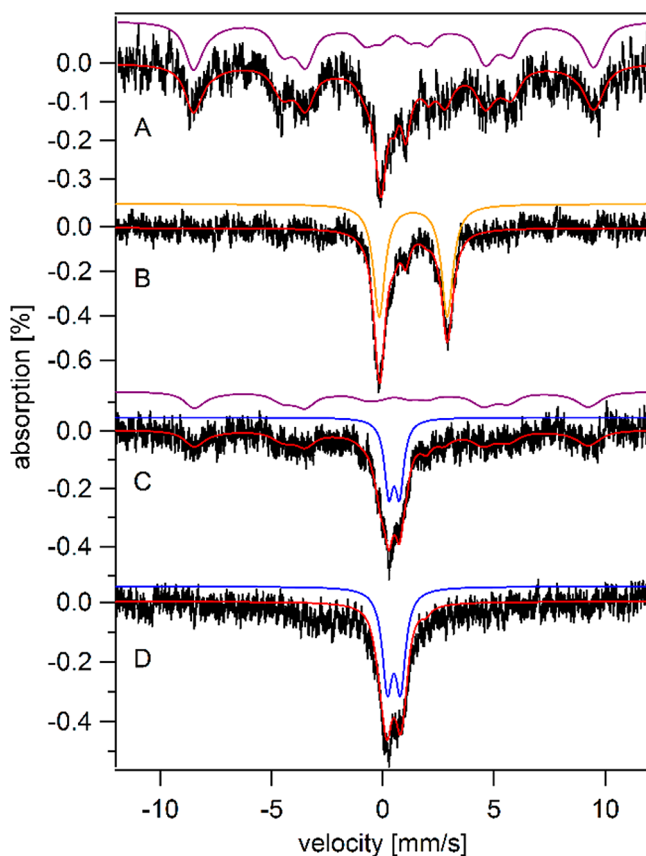


Figure 8. Five K, 0.05 T Mössbauer spectra of redox- and pH-perturbed lysates of MM cells harvested at $\text{OD}_{600} = 1.0$. (A) Cells before lysis. (B) Anaerobically lysed in 25 mM Tris-HCl and 1% Triton-X buffer (pH 7.4). (C) Lysed in a pure O₂ atmosphere using 0.5 M acetate and 1% Triton-X buffer (pH 4.5, final pH 5.0). (D) Same as (C) but using 0.5 M Tris-HCl rather than acetate (pH 7.8, final).

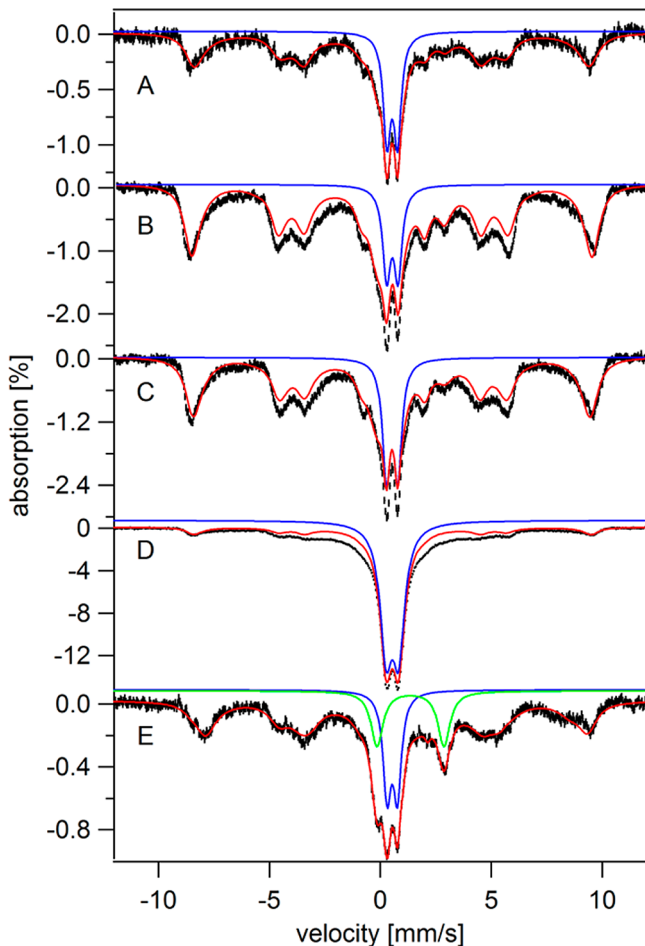


Figure 9. Five K 0.05 T Mössbauer spectra of cells grown for 5 days on different media. (A) G↓, (B) MM, (C) G↑, (D) G↑Fe↑, (E) R+. Red lines are composite simulations including the NHHS Fe^{III} sextet, the NHHS Fe^{II} and HS Fe^{II} heme doublets, the CD, and the Fe^{III} nanoparticle doublet. Blue and green lines are simulations of spectral features from Fe^{III} nanoparticle and NHHS Fe^{II}, respectively.

cells (Figure 10A) than in G↑ (Figure 10C) or MM (Figure 10B) cells. This makes sense because G↓ cells must rely on respiration for growth whereas G↑ (and MM) cells rely more on fermentation.³⁶

G↑ cells exhibited about 2-fold higher levels of oxidative damage relative to comparable MM-grown cells (Supporting Information Figure S3, compare lanes 2 vs 1 for 1-day growth and lanes 6 vs 5 for 5-day growth). Conversely, G↓ cells displayed only ca. 30% of the oxidative damage of comparable MM cells (Supporting Information Figure S4). These results are consistent with previous reports concluding that the level of oxidative stress in cells is proportional to the level of glycolysis.^{37–39}

We also grew G↑ cells in medium that contained 10 times the normal level of Fe (400 rather than 40 μM). Cells grown on this G↑Fe↑ medium contained nearly 3 times more Fe relative to cells grown on G↑ medium (Supporting Information Table S1). The 5 K Mössbauer spectra of G↑Fe↑ (Figure 9D) and Fe↑ cells (Figure 6A in ref 17) were dominated by nanoparticles (50–70% spectral intensity) and NHHS Fe^{III} (10–15% intensity). Thus, adding extra Fe to G↑ medium caused a massive increase of nanoparticles in the cell, again suggesting that the low-affinity Fe import rate is sensitive to the

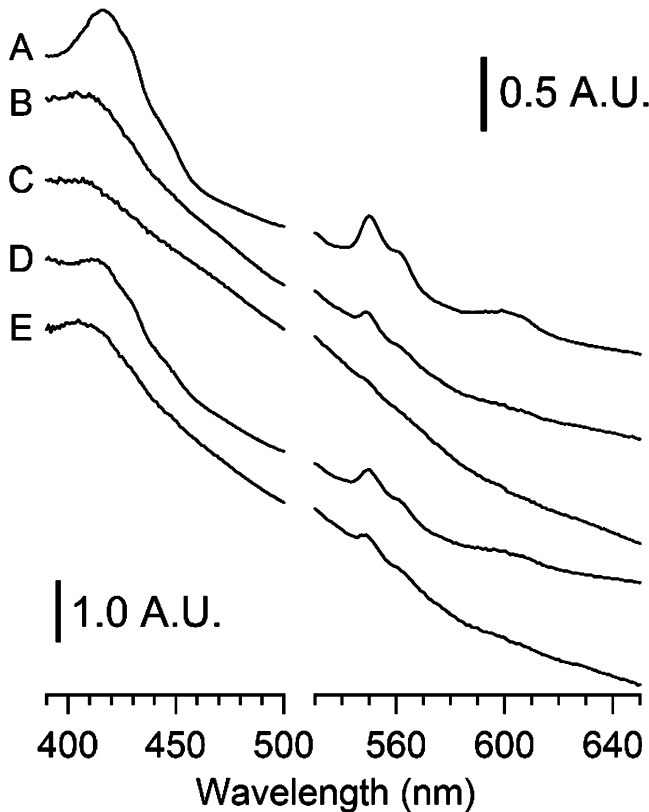


Figure 10. Electronic absorption spectra of 5-day-old cells grown on different media. (A) G↓, (B) MM, (C) G↑, (D) R+, (E) same as R+ medium but lacking rapamycin.

Fe concentration in the medium. This increase in nanoparticle buildup had no effect on the level of oxidative damage (Supporting Information Figure S3, compare lanes 3 vs 2 for 1-day growth and lanes 7 vs 6 for 5-day growth). Amazingly, the extent of oxidative damage suffered by the nanoparticle-packed G↑Fe↑ cells was about the same in G↑ cells despite the 3-fold greater concentration of Fe in G↑Fe↑ cells. Again, the extent of oxidative damage may depend on the cellular location of the nanoparticles.

Effect of Rapamycin. MM cells treated with rapamycin (R+ medium) grew slowly for 2 days, probably due to G0 arrest,³⁹ and then rapidly over the next 3 days such that 5-day-old R+ cells in stationary state had ca. 25% *higher* culture density than similarly aged MM cells (Supporting Information Table S1). The Fe concentration of 5-day-old R+ cells was ca. 6-fold *less* than that of MM-grown cells harvested at a similar age. This suggests that the Fe import rate of R+ cells at stationary state was significantly lower, relative to that of MM-grown cells, and better synchronized with the decline of growth rate as cells reached steady-state. A similar effect on Fe import rate was implicated in cells grown on G↓ medium. R+ cells exhibited a stronger heme signal compared with control (Figure 10D vs 10E), similar to the effect observed in G↓ cells. In this respect, rapamycin treatment (inhibiting the TOR system) and glucose deprivation exhibited similar cellular responses (less Fe accumulation and better postexponential Fe regulation), with the effect of rapamycin stronger than that of glucose.

The Mössbauer spectrum of R+ cells exhibited a more intense NHHS Fe^{II} doublet relative to that of MM cells (Figure 9E vs Figure 4E of ref 17). The parameters associated with it were within ±0.1 mm/s of those used to simulate the Fe^{II}_{ON}

doublet associated with A \downarrow cells and MM cell extracts. The percentage of magnetic Fe in the sample (affording the NHHS Fe III sextet and Fe III nanoparticle doublet) was comparable to that of MM-grown cells. However, because the overall Fe concentration was less, our results predict a decline in the magnetization of these cells. Indeed, inhibiting TORC1 lowers the magnetization in yeast cells.⁴⁰

Another interesting effect of inhibiting TORC1 was a reduced level of oxidative damage (Supporting Information Figure S3, lanes 4 and 8). The level of oxidative damage in 1-day-old R+ cells was 2–4 times less than in 1 day old cells grown on any other medium studied here. The extent of oxidative damage in 5-day-old R+ cells was also extremely low. In this respect, rapamycin treatment (i.e., TORC1 inhibition) and glucose deprivation again exhibited similar effects. In contrast, the extent of oxidative damage in G \uparrow cells was greatest of any condition studied.

■ DISCUSSION

Our results regarding adenine deficiency suggest the model shown in Figure 11. Here, the vacuoles of ADE2 Δ yeast cells grown on MM (Figure 11, top) are oxidizing and acidic, such that the Fe in these organelles is predominately mononuclear NHHS Fe III (but with some nanoparticles). The redox status of the vacuoles is maintained by the import of GSSG via Ycf1p into the vacuolar lumen. This process maintains a high ratio of GSH/GSSG in the cytosol, resulting in a cytosolic redox potential of ca. -320 mV.²⁴ The redox state of vacuolar Fe is controlled by the reaction $2\text{Fe}^{\text{II}} + \text{GSSG} + 2\text{H}^+ \rightleftharpoons 2\text{GSH} + 2\text{Fe}^{\text{III}}$. Reduced GSH generated in this way is pumped into the cytosol. The vacuoles are acidic, stimulating Fe $^{\text{II}}$ oxidation, but the pH is high enough that a small proportion of mononuclear NHHS Fe III species is converted into nanoparticles. The redox potential is such that a small proportion of the Fe pool remains as Fe $^{\text{II}}$.

The vacuoles of cells grown on A \downarrow medium are similarly configured during exponential growth. However, as the medium become depleted of adenine, the cells express the enzymes of the adenine biosynthetic pathway (Figure 11, middle). Due to the absence of ADE2, this is a futile effort, and the adenine deficiency prompts the cells to transition earlier into stationary state. The toxic intermediate AIR accumulates and the cell sequesters it by forming a GS-AIR conjugate that is pumped into vacuoles via Ycf1p, *the same membrane-bound protein that pumps GSSG into vacuoles under adenine-sufficient conditions*. Due to this competition, GSSG import becomes partially blocked, causing these organelles to become more reducing than they are under MM growth conditions. The majority of the vacuolar Fe III becomes reduced to the Fe $^{\text{II}}$ state, with Fe $^{\text{II}}_{\text{ON}}$ and Fe $^{\text{II}}_{\text{ONS}}$ species dominating.

As cells stop growing, they stop producing AIR, such that GSSG can again be imported into vacuoles, thereby reestablishing normal oxidized conditions. This explains the transient nature of the observed adenine-deficiency effect. Fe $^{\text{II}}_{\text{ON/NS}}$ reoxidize to the Fe III state, including both HS Fe III and Fe III nanoparticles. Vacuolar pH might also increase in stationary state cells,⁴¹ promoting nanoparticle formation.

Fe $^{\text{II}}_{\text{ON}}$ and Fe $^{\text{II}}_{\text{ONS}}$ may coexist with NHHS Fe III in the vacuole, or one or both may be exported into the cytosol. Our previous model¹³ posits that once vacuolar Fe III is reduced to Fe $^{\text{II}}$, it immediately exits the vacuole and moves into the cytosol. This model was based on the lack of HS Fe $^{\text{II}}$ in isolated vacuoles. Fe $^{\text{II}}$ in vacuoles may be exported via Smf3p, a divalent

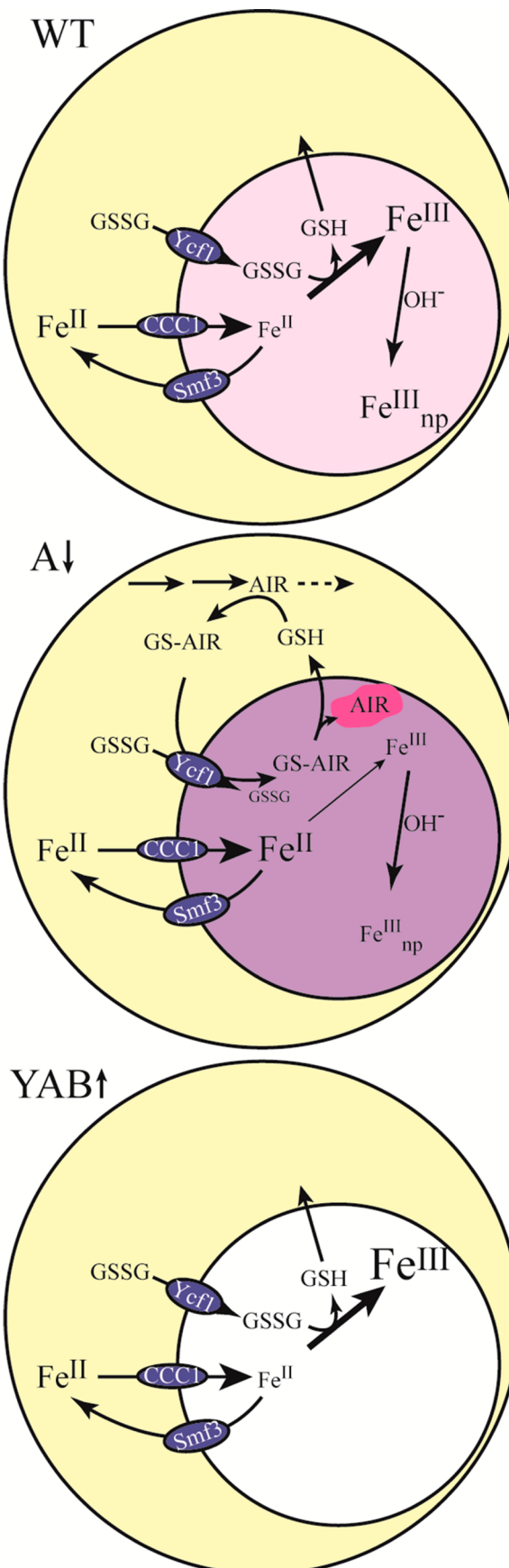


Figure 11. Model for the Fe status in yeast vacuole according to the different media conditions. Top, MM; middle, A \downarrow ; bottom, YAB \uparrow . See text for details.

metal transporter located on the vacuolar membrane,⁶ as well as via Fth1p/Fet5p.⁴² Our current MB studies show that vacuoles isolated from adenine-deficient cells also lacked NHHS Fe^{II} species, again suggesting that Fe^{II}_{ON} and Fe^{II}_{ONS} are located in the cytosol. However, we have also found that Fe *leaches* from vacuoles during isolation, consistent with our preferred speculation that Fe^{II}_{ONS} is located in vacuoles within adenine-deficient cells and that Fe^{II}_{ON} is in the cytosol. This possibility needs to be investigated further.

Vacuoles in chronologically older YAB↑ cells are more acidic than in equivalent MM cells (Figure 11, bottom). This prevents nanoparticles from forming and causes mononuclear NHHS Fe^{III} to accumulate instead. We view this loosely as YAB↑ medium keeping cells “younger”, with more acidic vacuoles. An increase in vacuolar pH in aged cells is known to limit mitochondrial function, which possibly implies lower levels of ISCs and hemes in older cells.⁴¹ Consistent with this, YAB↑ cells, although grown for 5 days, afforded higher mitochondrial heme levels than equivalent MM cells. Increased vacuolar pH also inhibits synthesis of long-chain polyphosphates,⁴³ which might be ligands of vacuolar Fe^{III}.¹³ Thus, the shift toward nanoparticles at high vacuolar pH may also be related to changes in polyphosphate concentrations.

Glucose. The effect of glucose on yeast Fe metabolism suggests that the low-affinity Fe importer (probably involving Fet4p or Smf1p)^{5,6} is regulated (directly or indirectly) by the glucose concentration in the cell. Glucose levels may affect ATP levels, which may affect Fe import processes at the plasma membrane. High glucose concentrations *increase* the rate of postexponential Fe import, whereas lower glucose concentrations *decrease* it. Because glucose concentrations do not affect the rate of cell growth, this leads to an accumulation of Fe in the cell under high glucose levels. Glucose also represses cellular respiration,³⁶ which explains the decline of ISCs and heme centers that are generally associated with mitochondria. The extent of oxidative stress is also modulated by the initial level of glucose in media. The more glucose, the more the cells are oxidatively stressed.

Similar effects of glucose on the Fe concentration and oxidative stress of cells have been reported by Reverte-Branchat et al.³⁷ They grew cells on rich media supplemented with 2% (w/v) and 0.5% (w/v) glucose and monitored for [Fe] and oxidative stress for two months and 16–18 generations. They observed stronger oxidative stress and higher [Fe] in cells fed more glucose. They concluded that the pro-oxidant effects due to the increased Fe caused the enhanced damage. We demonstrated here that oxidative stress is *not* directly related to the level of cellular Fe but more closely related to glucose metabolism. How glucose promotes ROS generation in yeast is not known, but multiple biochemical pathways in which glucose metabolism can generate ROS in mammalian cells have been reported, including glyceraldehyde autoxidation, protein kinase C activation and oxidative phosphorylation.⁴⁴ Glucose suppresses a nutrient-dependent protein kinase (Rim15p) that regulates expression of genes involved in antioxidant defense, e.g., *SOD1* and *SOD2*, thereby increasing cellular ROS damage.⁴⁵

Rapamycin. The effect of rapamycin is roughly the opposite of glucose. Lowering TORC1 activity by rapamycin treatment or knockout of Tco89p, a component of TORC1, reduces the magnetization of yeast grown on high Fe-containing media, arrests growth at G0 and increases respiration.^{25,38,40} Consistent with those reports, we found that rapamycin

inhibited the rates of Fe import and cell growth (prompting a lag period prior to exponential growth) and it promoted respiration. These effects appear opposite of those caused by glucose. Unlike glucose, rapamycin altered the distribution and speciation of cellular Fe. Rapamycin shifted the vacuole to more reducing (and perhaps more basic) conditions. Similar effects have been reported in the Tco89p knockout strain,⁴⁰ allowing the presence of Fe^{II} together with some Fe^{III} nanoparticles.

The rapamycin effect is consistent with previous reports that rapamycin increases life span in many organisms including yeast.²⁵ The increased final OD₆₀₀ by rapamycin treatment relative to that of MM cells implies an extended replicative life span as does the decreased level of oxidative damage. Also, the reducing cellular environment associated with rapamycin treatment supports a model in which reduced TORC1 activity increases chronological life span by increasing Rim15p-dependent and Rim15p-independent expression of environmental stress-response genes.^{46–48}

In summary, we have found that the concentration, speciation and distribution of Fe in yeast are altered dramatically by changing the composition of nutrients in the growth medium. This illustrates the complex connections between nutrient composition, cellular metabolism, and Fe speciation in the cell. Our results demonstrate the importance of vacuolar redox status and pH in controlling the form(s) of Fe contained in these organelles. Vacuolar Fe is not “locked” into a particular redox state or chemical form, but it exhibits substantial redox chemistry and ligand-exchange reactions, and is influenced quite sensitively by cellular metabolic processes. Along with the mitochondria, vacuoles are a major “hub” for Fe trafficking. Thus, deciphering the chemistry of Fe in vacuoles will be essential for a more comprehensive molecular-level understanding of iron metabolism in yeast cells, the predominant eukaryotic “workhorse” that leads advances in this field.

ASSOCIATED CONTENT

Supporting Information

Figure S1, 5 K, 0.05 T Mössbauer spectrum of another batch of yeast cells grown for 5 days on A↓; Figure S2, UV-vis spectra of whole yeast cells grown for 5 days on MM and YAB↑; Figure S3, Oxyblot assay of whole cells grown on different media and harvested during different phases; Figure S4, Oxyblot assay of whole cells grown on MM and G↓; Table S1, Final OD₆₀₀ and [Fe_{cell}] after 5 days of growth on various media; Table S2. Mössbauer parameters determined from the spectra listed in the main text and Supporting Information. This material is available free of charge via the Internet at <http://pubs.acs.org>.

AUTHOR INFORMATION

Corresponding Author

*E-mail: Lindahl@chem.tamu.edu. Phone: 979-845-0956. Fax: 979-845-4719.

Present Address

[†]Nuclear Chemistry Research Division, Korea Atomic Energy Research Institute, Daejeon, 305–353, Republic of Korea

Funding

This study was funded by the National Institutes of Health (GM084266) and the Robert A. Welch Foundation (A1170).

Notes

The authors declare no competing financial interest.

ACKNOWLEDGMENTS

We thank Brad Pierce (University of Texas, Arlington) for allowing us to use his EPR spectrometer.

ABBREVIATIONS

AIR, phosphoribosylaminoimidazole; CD, central doublet; DMSO, dimethyl sulfoxide; EPR, electron paramagnetic resonance; G↑, MM-based medium in which the concentration of glucose was 3X higher than in MM; G↑Fe↑, same as G↑ but with 10-fold higher concentration of ferric citrate in the medium; G↓, MM-based medium in which the concentration of glucose was 10X lower than in MM; GSSG, oxidized glutathione disulfide; GSH, reduced glutathione; HS, high spin; ICP-MS, inductively coupled plasma mass spectrometry; ISC, iron sulfur cluster; MB, Mössbauer; MM, minimal medium; NHHS, nonheme high spin; OD, optical density; R+, MM medium plus rapamycin; ROS, reactive oxygen species; SDS, sodium dodecyl sulfate; SOD2, superoxide dismutase 2; TOR, target of rapamycin; TORC1, TOR complex 1; WT, wild type; YAB↑, a MM-based medium in which the concentrations of YNB, amino acids Leu, His, and Trp and nucleotide bases adenine and uracil were increased 3-fold; YNB, yeast nitrogen base

REFERENCES

- (1) Crichton, R. R. (2008) in *Biological Inorganic Chemistry*, pp 211–240, Elsevier, Amsterdam.
- (2) Van Ho, A., Ward, D. M., and Kaplan, J. (2002) Transition metal transport in yeast. *Annu. Rev. Microbiol.* 56, 237–261.
- (3) Lill, R., and Mühlhoff, U. (2008) Maturation of iron-sulfur proteins in eukaryotes: Mechanisms, connected processes, and diseases. *Annu. Rev. Biochem.* 77, 669–700.
- (4) Stearman, R., Yuan, D. S., Yamaguchi-Iwai, Y., Klausner, R. D., and Dancis, A. (1996) A permease-oxidase complex involved in high-affinity iron uptake in yeast. *Science* 271, 1552–1557.
- (5) Dix, D. R., Bridgman, J. T., Broderius, M. A., Byersdorfer, C. A., and Eide, D. J. (1994) The FET4 gene encodes the low-affinity Fe(II) transport protein of *Saccharomyces cerevisiae*. *J. Biol. Chem.* 269, 26092–26099.
- (6) Portnoy, M. E., Liu, X. F., and Culotta, V. C. (2000) *Saccharomyces cerevisiae* expresses three functionally distinct homologues of the Nramp family of metal transporters. *Mol. Cell. Biol.* 20, 7893–7902.
- (7) Shakoury-Elizeh, M., Tiedeman, J., Rashford, J., Ferea, T., Demeter, J., Garcia, E., Rolfs, R., Brown, P. O., Botstein, D., and Philpott, C. C. (2004) Transcriptional remodeling in response to iron deprivation in *Saccharomyces cerevisiae*. *Mol. Biol. Cell* 15, 1233–1243.
- (8) Li, H., Mapolelo, D. T., Dingra, N. N., Keller, G., Riggs-Gelasco, P. J., Winge, D. R., Johnson, M. K., and Outten, C. E. (2011) Histidine 103 in Fra2 is an iron-sulfur cluster ligand in the [2Fe-2S] Fra2-Grx3 complex and is required for in vivo iron signaling in yeast. *J. Biol. Chem.* 286, 867–876.
- (9) Ueta, R., Fujiwara, N., Iwai, K., and Yamaguchi-Iwai, Y. (2012) Iron-induced dissociation of the Aft1p transcriptional regulator from target gene promoters is an initial event in iron-dependent gene suppression. *Mol. Cell. Biol.* 32, 4998–5008.
- (10) Froschauer, E. M., Schweyen, R. J., and Wiesenberger, G. (2009) The yeast mitochondrial carrier proteins Mrs3p/Mrs4p mediate iron transport across the inner mitochondrial membrane. *BBA, Biophys. Acta, Biomembr.* 1788, 1044–1050.
- (11) Mühlhoff, U., Stadler, J. A., Richhardt, N., Seubert, A., Eickhorst, T., Schweyen, R. J., Lill, R., and Wiesenberger, G. (2003) A specific role of the yeast mitochondrial carriers Mrs3/4p in mitochondrial iron acquisition under iron-limiting conditions. *J. Biol. Chem.* 278, 40612–40620.
- (12) Brett, C. L., Kallay, L., Hua, Z., Green, R., Chyou, A., Zhang, Y., Graham, T. R., Donowitz, M., and Rao, R. (2011) Genome-wide analysis reveals the vacuolar pH-stat of *Saccharomyces cerevisiae*. *PLoS One* 6, e17619.
- (13) Cockrell, A. L., Holmes-Hampton, G. P., McCormick, S. P., Chakrabarti, M., and Lindahl, P. A. (2011) Mössbauer and EPR study of iron in vacuoles from fermenting *Saccharomyces cerevisiae*. *Biochemistry* 50, 10275–10283.
- (14) Holmes-Hampton, G. P., Jhurry, N. D., McCormick, S. P., and Lindahl, P. A. (2013) Iron content of *Saccharomyces cerevisiae* cells grown under iron-deficient and iron-overload conditions. *Biochemistry* 52, 105–114.
- (15) Milgrom, E., Diab, H., Middleton, F., and Kane, P. M. (2007) Loss of vacuolar proton-translocating ATPase activity in yeast results in chronic oxidative stress. *J. Biol. Chem.* 282, 7125–7136.
- (16) Diab, H. I., and Kane, P. M. (2013) Loss of vacuolar H⁺-ATPase (V-ATPase) activity in yeast generates an iron deprivation signal that is moderated by induction of the peroxiredoxin TSA2. *J. Biol. Chem.* 288, 11366–11377.
- (17) Park, J., McCormick, S. P., Chakrabarti, M., and Lindahl, P. A. (2013) Lack of synchronization between iron uptake and cell growth leads to iron overload in *Saccharomyces cerevisiae* during post-exponential growth modes. *Biochemistry* 52, 9413–9425.
- (18) Smirnov, M. N., Smirnov, V. N., Budowsky, E. I., Ingvechtomov, S. G., and Serebrjakov, N. G. (1967) Red pigment of adenine-deficient yeast *Saccharomyces cerevisiae*. *Biochem. Biophys. Res. Commun.* 27, 299–304.
- (19) Sharma, K. G., Kaur, R., and Bachhawat, A. K. (2003) The glutathione-mediated detoxification pathway in yeast: an analysis using the red pigment that accumulates in certain adenine biosynthetic mutants of yeasts reveals the involvement of novel genes. *Arch. Microbiol.* 180, 108–117.
- (20) Chaudhuri, B., Ingavale, S., and Bachhawat, A. K. (1997) *apd1*(+), a gene required for red pigment formation in *ade6* mutants of *Schizosaccharomyces pombe*, encodes an enzyme required for glutathione biosynthesis: A role for glutathione and a glutathione-conjugate pump. *Genetics* 145, 75–83.
- (21) Sharma, K. G., Mason, D. L., Liu, G. S., Rea, P. A., Bachhawat, A. K., and Michaelis, S. (2002) Localization, regulation, and substrate transport properties of Bpt1p, a *Saccharomyces cerevisiae* MRP-type ABC transporter. *Eukaryotic Cell* 1, 391–400.
- (22) Mehdi, K., Thierie, J., and Penninckx, M. J. (2001) γ -glutamyl transpeptidase in the yeast *Saccharomyces cerevisiae* and its role in the vacuolar transport and metabolism of glutathione. *Biochem. J.* 359, 631–637.
- (23) Toledano, M. B., Delaunay-Moisan, A., Outten, C. E., and Igbaria, A. (2013) Functions and cellular compartmentation of the thioredoxin and glutathione pathways in yeast. *Antioxid. Redox Signaling* 18, 1699–1711.
- (24) Morgan, B., Ezerina, D., Amoako, T. N. E., Riemer, J., Seedorf, M., and Dick, T. P. (2013) Multiple glutathione disulfide removal pathways mediate cytosolic redox homeostasis. *Nat. Chem. Biol.* 9, 119–125.
- (25) Loewith, R., and Hall, M. N. (2011) Target of rapamycin (TOR) in nutrient signaling and growth control. *Genetics* 189, 1177–1201.
- (26) Park, J., McCormick, S. P., Chakrabarti, M., and Lindahl, P. A. (2013) Insights into the iron-ome and manganese-ome of $\Delta mtm1$ *Saccharomyces cerevisiae* mitochondria. *Metalomics* 5, 656–672.
- (27) Miao, R., Kim, H., Koppolu, U. M. K., Ellis, E. A., Scott, R. A., and Lindahl, P. A. (2009) Biophysical characterization of the iron in mitochondria from Atm1p-depleted *Saccharomyces cerevisiae*. *Biochemistry* 48, 9556–9568.
- (28) Miao, R., Holmes-Hampton, G. P., and Lindahl, P. A. (2011) Biophysical investigation of the iron in Aft1-1(up) and Gal-YAH1 *Saccharomyces cerevisiae*. *Biochemistry* 50, 2660–2671.
- (29) Silver, J., Hamed, M. Y., and Morrison, I. E. G. (1985) Studies of the reactions of ferric iron with glutathione and some related thiols.

- Part V. Solid complexes containing Fe^{II} and glutathione or Fe^{III} with oxidized glutathione. *Inorg. Chim. Acta* 107, 169–178.
- (30) Roach, P. L., Clifton, I. J., Hensgens, C. M. H., Shibata, N., Schofield, C. J., Hajdu, J., and Baldwin, J. E. (1997) Structure of isopenicillin N synthase complexed with substrate and the mechanism of penicillin formation. *Nature* 387, 827–830.
- (31) Chen, V. J., Orville, A. M., Harpel, M. R., Frolik, C. A., Surerus, K. K., Münck, E., and Lipscomb, J. D. (1989) Spectroscopic studies of isopenicillin N synthase. A mononuclear nonheme Fe²⁺ oxidase with metal coordination sites for small molecules and substrate. *J. Biol. Chem.* 264, 21677–21681.
- (32) Stevens, B. J. (1977) Variation in number and volume of mitochondria in yeast according to growth-conditions - Study based on serial sectioning and computer graphics reconstitution. *Biol. Cell.* (1977-1980) 28, 37–56.
- (33) Lesuisse, E., Santos, R., Matzanke, B. F., Knight, S. A. B., Camadro, J.-M., and Dancis, A. (2003) Iron use for haeme synthesis is under control of the yeast frataxin homologue (Yfh1). *Hum. Mol. Genet.* 12, 879–889.
- (34) Miao, R., Martinho, M., Morales, J. G., Kim, H., Ellis, E. A., Lill, R., Hendrich, M. P., Münck, E., and Lindahl, P. A. (2008) EPR and Mössbauer spectroscopy of intact mitochondria isolated from Yah1p-depleted *Saccharomyces cerevisiae*. *Biochemistry* 47, 9888–9899.
- (35) Kosman, D. J. (2003) Molecular mechanisms of iron uptake in fungi. *Mol. Microbiol.* 47, 1185–1197.
- (36) Broach, J. R. (2012) Nutritional control of growth and development in yeast. *Genetics* 192, 73–105.
- (37) Reverter-Branchat, G., Cabisco, E., Tamarit, J., and Ros, J. (2004) Oxidative damage to specific proteins in replicative and chronological-aged *Saccharomyces cerevisiae*—Common targets and prevention by calorie restriction. *J. Biol. Chem.* 279, 31983–31989.
- (38) Bonawitz, N. D., Chatenay-Lapointe, M., Pan, Y., and Shadel, G. S. (2007) Reduced TOR signaling extends chronological life span via increased respiration and upregulation of mitochondrial gene expression. *Cell Metab.* 5, 265–277.
- (39) Barbet, N. C., Schneider, U., Hellwell, S. B., Stansfield, I., Tuite, M. F., and Hall, M. N. (1996) TOR controls translation initiation and early G1 progression in yeast. *Mol. Biol. Cell* 7, 25–42.
- (40) Nishida, K., and Silver, P. A. (2012) Induction of biogenic magnetization and redox control by a component of the target of rapamycin complex 1 signaling pathway. *PLoS Biol.* 10, e1001269.
- (41) Hughes, A. L., and Gottschling, D. E. (2012) An early age increase in vacuolar pH limits mitochondrial function and lifespan in yeast. *Nature* 492, 261–265.
- (42) Portnoy, M. E., Jensen, L. T., and Culotta, V. C. (2002) The distinct methods by which manganese and iron regulate the Nramp transporters in yeast. *Biochem. J.* 362, 119–124.
- (43) Trilisenko, L., Tomashevsky, A., Kulakovskaya, T., and Kulaev, I. (2013) V-ATPase dysfunction suppresses polyphosphate synthesis in *Saccharomyces cerevisiae*. *Folia Microbiol. (Dordrecht, Neth.)* 58, 437–441.
- (44) Robertson, R. P. (2004) Chronic oxidative stress as a central mechanism for glucose toxicity in pancreatic islet beta cells in diabetes. *J. Biol. Chem.* 279, 42351–42354.
- (45) Cameroni, E., Hulo, N., Roosen, J., Winderickx, J., and Virgilio, C. D. (2004) The novel yeast PAS kinase Rim15 orchestrates G0-associated antioxidant defense mechanisms. *Cell Cycle* 3, 460–466.
- (46) Wanke, V., Cameroni, E., Uotila, A., Piccolis, M., Urban, J., Loewith, R., and De Virgilio, C. (2008) Caffeine extends yeast lifespan by targeting TORC1. *Mol. Microbiol.* 69, 277–285.
- (47) Wei, M., Fabrizio, P., Hu, J., Ge, H., Cheng, C., Li, L., and Longo, V. D. (2008) Life span extension by calorie restriction depends on Rim15 and transcription factors downstream of Ras/PKA, Tor, and Sch9. *PLoS Genet.* 4, e13.
- (48) Pan, Y., Schroeder, E. A., Ocampo, A., Barrientos, A., and Shadel, G. S. (2011) Regulation of yeast chronological life span by TORC1 via adaptive mitochondrial ROS signaling. *Cell Metab.* 13, 668–678.